frontiers | Frontiers in Marine Science

TYPE Original Research
PUBLISHED 17 March 2023
DOI 10.3389/fmars.2023.1085345

OPEN ACCESS

EDITED BY
John Lee Ferry,
University of South Carolina, United States

REVIEWED BY
Ana Soares,
Cranfield University, United Kingdom
Rahul Nitnavare,
Rothamsted Research, United Kingdom

*CORRESPONDENCE
Dao-Feng Zhang
zdf@hhu.edu.cn
Chuang Liu
20190099@hhu.edu.cn

SPECIALTY SECTION
This article was submitted to Marine Biogeochemistry, a section of the journal Frontiers in Marine Science

RECEIVED 03 November 2022
ACCEPTED 23 February 2023
PUBLISHED 17 March 2023

CITATION
He W, Xue H-P, Liu C, Zhang AH, Huang J-K and Zhang D-F (2023) Biomineralization of struvite induced by indigenous marine bacteria of the genus *Alteromonas*. *Front. Mar. Sci.* 10:1085345. doi: 10.3389/fmars.2023.1085345

Biomineralization of struvite induced by indigenous marine bacteria of the genus *Alteromonas*

Wei He, Hua-Peng Xue, Chuang Liu*, Ai Hua Zhang, Jian-Ke Huang and Dao-Feng Zhang*

Institute of Marine Biotechnology and Bio-resource Utilization, College of Oceanography, Hohai University, Nanjing, China

Biomineralization is a universal phenomenon in the ocean that plays an important role in marine geochemical circulation. The genus *Alteromonas* is an indigenous taxon with a wide distribution and various ecological roles in the ocean, but biomineralization by this genus has not been reported. In this study, five *Alteromonas* spp. were found to induce mineral crystal formation of different shapes and sizes in agar media. Further studies on deep-sea strains *A. alteriprofundi* HHU 13199^{T} and *A. alterisediminis* N102^{T} showed that they could produce mineral crystals with similar morphology when grown in agar or broth media with different concentrations of sea salts (i.e., 2%, 4%, 6%, and 8%), and that their growth was dependent on Ca^{2+} and/or Mg^{2+} ion concentrations. Genomic analysis showed that the genus *Alteromonas* universally possessed the ammonification metabolism pathway and that, during the culture of these bacteria, the production of mineral crystals was accompanied by an increase in ammonia concentration and pH value and a decrease in nitrate nitrogen concentration. The addition of ammonia to broth media (≈ 572.7 mg/L) simulated the ammonia content in media on days 5 and 6 of bacterial growth and also induced mineral crystals to form. Through the analysis using scanning electron microscope–energy-dispersive spectrometry (SEM-EDS), X-ray diffraction (XRD), Fourier-transform infrared microscopy (FTIR), thermogravimetric (TG) analysis, and differential thermal gravity and differential scanning calorimetry (DTG–DSC), mineral crystals induced by bacterial strains and the non-strain (ammonia-added sample) were all identified as struvite mineral. In addition, the characteristics of the struvite mineral induced by bacterial strains were different from the characteristics of the struvite synthesized by non-strain and of a struvite mineral standard. Thus, this study deduces that *Alteromonas* spp. possess the ability to induce struvite formation. The mechanism mainly lies in the presence of an ammonification metabolism pathway to produce ammonia, which should be recognized as biologically induced mineralization (BIM). This study provides insight into a new ecological role of indigenous marine taxa of the genus *Alteromonas*.

KEYWORDS

***Alteromonas*, biomineralization, struvite, nitrate reduction, ammonia**

1 Introduction

Oceans and seas are composed of 96.7% water and 3.3% dissolved salts; almost all elements in the periodic table can be found in seawater, although many occur at very low concentrations (Loganathan et al., 2017). Many ions, which make up salts, are essential micronutrients for microbial growth, and are able to participate in biological processes inside the cells, such as coenzyme reactions, redox reactions, and osmotic regulation (Nies, 1999; Bruins et al., 2000). From a different perspective, marine microorganisms possess unique properties owing to the need to adapt to disadvantageous environmental conditions caused by ions, such as alkaline and acidic water, and high osmotic stress. For example, microorganisms can change the valence, existence form, and solubility of the ion (Beam et al., 2018; Vigliaturo et al., 2020; Sanz-Saez et al., 2022; van de Velde et al., 2022).

Biomineralization is the biological process in which organisms deposit associated ions by raising the pH around cells to supersaturate mineral ion concentrations (Han et al., 2015; Falagán et al., 2017). The formation of minerals and rocks is also closely related to biomineralization; for example, some aerobic bacteria can induce the formation of dolomite, calcium magnesium carbonate, and high-magnesium calcite (Deng et al., 2010; Li et al., 2017). In addition, some microorganisms in hypersaline brackish lakes can induce the deposition of Ca^{2+} and Mg^{2+} ions to form modern carbonate stromatolites (Spadafora et al., 2010). Based on biological control, biomineralization is currently categorized into three distinct groups (Park and Faivre, 2022): (i) biologically influenced biomineralization (BFM), a passive mineralization process depending on negatively charged molecules on the cell surface, such as proteins, lipids, and glycoproteins on the bacterial cell wall and extracellular polymeric substances (EPS); (ii) biologically induced biomineralization (BIM) (Frankel and Bazylinski, 2003), which depends on inorganic materials in the environment driven by cellular activities that change the chemical composition of the cell's interstitial space, resulting in a high-pH microenvironment, such as photosynthesis, urea hydrolysis, nitrate reduction, deamination, and sulfate reduction; and (iii) biologically controlled biomineralization (BCM), associated with an organic matrix that forms an isolated intracellular environment and refers to the precipitation of minerals by elaborate cellular control. Many microbial taxa have been reported to possess biomineralization capabilities, some of which have been used in wastewater treatment (Han et al., 2014; Ronholm et al., 2014; Han et al., 2015; Sun et al., 2020; Leng and Soares, 2021; Zhang et al., 2022). There is a large variety and wide distribution of bacteria in oceans and seas. Therefore, it is of great research significance to study the biomineralization by microorganisms in the ocean for the regulation of metal ions in seawater.

Alteromonas spp. are widespread, abundant, and phytoplankton-associated indigenous marine copiotrophs, and live in a variety of habitats, especially the seawaters from the tropics to the poles, and even hadal zones (Ivars-Martinez et al., 2008; Gonzaga et al., 2012; Gago et al., 2021). The Tara Oceans expedition found that *Alteromonas* had an occurrence rate reaching 80%, with consistently high relative abundances (Nayfach et al., 2016). In phytoplankton blooms of the western North Pacific Ocean, members of the genus *Alteromonas* contributed to the total bacterial biomass as much as the *Cytophaga–Flavobacterium–Bacteroides* (CFB) group and *Roseobacter* (Tada et al., 2011; Sarmento and Gasol, 2012). In the Challenger Deep of the Mariana Trench, *Alteromonas* was found to still be abundant, with a 16S rRNA gene proportion > 5% of the microbial community across the near-bottom water (> 10,000 m below the surface and ≈ 300–400 m from the seafloor) (Liu et al., 2019). Metatranscriptomic studies have shown *Alteromonas* to be a key member of global ocean carbon and nitrogen cycling, because of their strong capability to recycle dissolved organic carbon (McCarren et al., 2010; Pedler et al., 2014). In addition, *Alteromonas* strains have also been found to make significant contributions to marine iron cycling and transport, and many gene clusters have been identified to be involved with resistance to heavy metals (Debeljak et al., 2019; Manck et al., 2020; Cusick et al., 2021; Zhang et al., 2021). It has also been reported that *Alteromonas* spp. produce extracellular polysaccharides (EPSs), enzymes, and secondary metabolites that have been used for biotechnological purposes with different applications (Lelchat et al., 2015; Zykwinska et al., 2018; Lee and Jun, 2019). Overall, the genus *Alteromonas* possesses great potential in applications of the biotechnological industry and plays important roles in the geochemical cycling of oceans.

The genus *Alteromonas* currently includes 35 validly published species (https://lpsn.dsmz.de/genus/alteromonas) (Parte et al., 2020), including five transferred from the genus *Salinimonas* for the consistent monophyletic nature of members of the two genera (Gago et al., 2021). During the taxonomic identification of *A. alteriprofundi* (= *S. profundi*) (Zhang et al., 2021), we found that this strain and its four close relatives, *A. alterisediminis* (= *S. sediminis*), *A. chungwhensis* (= *S. chungwhensis*), *A. iocasae* (= *S. iocasae*), and *A. lutimaris* (= *S. lutimaris*), could consistently produce macroscopic crystals in agar media. Although *Alteromonas* spp. are versatile in marine environments and have applications in the biotechnology industry, as suggested above, their biomineralization function has not been reported. Here, we further characterize crystals induced by these five *Alteromonas* spp., and provide insight into the related mechanism. This study suggested the potential involvement of species of the genus *Alteromonas* in marine struvite deposition and sheds new light on their ecological roles in marine environments.

2 Materials and methods

2.1 Bacterial strains and culture conditions

The experiments were performed with five strains of the genus *Alteromonas*: *A. alterisediminis* N102^T, isolated from deep-sea (4,700 m) sediment of the New Britain Trench (Cao et al., 2018); *A. alteriprofundi* HHU 13199^T, isolated from a marine sediment sample from the South China Sea at a depth of 2,918 m (Zhang et al., 2021); *A. chungwhensis* KCTC 12239^T, isolated from a solar saltern in South Korea (Jeon et al., 2005); *A. iocasae* MCCC 1K03884^T, isolated from a polychaete tube in a hydrothermal field of the Okinawa Trough (Zhang et al., 2020); and *A. lutimaris* KCTC 23464^T, isolated from a tidal flat on the southern

coast of South Korea (Yoon et al., 2012). These strains were maintained on 2216E medium (Solarbio, Beijing, China) and stored in aqueous glycerol suspensions (20%, v/v; volume to volume) at –80°C.

2.2 Sea salt dependence during bacterial growth

As previously reported, *A. alteriprofundi* HHU 13199^T could not be grown in tryptic soy agar (TSA, Bacto^{TM}) media supplemented with 2.5% NaCl (w/v), whereas the other four strains could (Jeon et al., 2005; Yoon et al., 2012; Cao et al., 2018; Zhang et al., 2020; Zhang et al., 2021). In this study, four different types of TSA media with Backhaus artificial seawater (ASW) of incomplete formula (I–IV, Table S1) were prepared to clarify which mineral salts were necessary and/or advantageous for bacteria growth. The TSA I–IV media contained (per liter): 10.0 g of tryptone, 5.0 g of soya peptone, 481 mM NaCl, and incomplete ASW I–IV. To clarify the optimal quantity, different concentrations (i.e., 0–1× of the original formula, at 0.1× intervals) of $CaCl_2$ (0–1.379 g/L) and $MgCl_2{\cdot}6H_2O$/$MgSO_4{\cdot}7H_2O$ (0–12.291 g/L), respectively, were supplemented with tryptic soy broth (TSB) media to determine the optimal additive amount. In addition, salinity differences of the original ASW formula for each treatment were eliminated by adding the corresponding weight of NaCl. A control group with no bacterial incubation was set up for each concentration. Bacterial growth was monitored by an automatic growth curve analyzer (Bioscreen C Pro; OY Growth Curves Ab Ltd, Helsinki, Finland), and measurements were taken every 2 hours.

2.3 Changes in pH, ammonia nitrogen and nitrate nitrogen during bacterial growth

The 2216E broth was used to monitor changes in pH, ammonia nitrogen (NH_3-N), and nitrate nitrogen (NO_3-N) during bacterial growth because it is oligotrophic and contains levels of nutrients much closer to the real marine environment than TSB. The initial pH of the 2216E broth was adjusted to 7.5 with 0.5 M NaOH and 0.5 M HCl solutions. The bacteria were inoculated into a volume of 500 mL of 2216E broth using a conical flask of 1,000 mL (2216E broth with no bacterial incubation was used as a control), cultured at 28°C for 120 hours with vibration (180 rpm), and sampled (30 mL) at 24-hour intervals. The samples were centrifuged at 6,000 × *g* for 10 minutes to obtain the supernatant. The pH value of the supernatant was measured using a water quality tester (PHSJ-4F; Oustor, Shanghai, China). NH_3-N content was determined by Nessler's reagent spectrophotometry (Gao et al., 2018). NO_3-N content was determined by alkaline potassium persulfate digestion followed by UV spectrophotometry (Purcell and King, 1996).

2.4 Mineral crystallization and isolation

Mineral crystallization was investigated by incubating bacteria in TSA/TSB (Difco) supplemented with 3.0% (w/v) sea salt media and 2216E broth for 10 days, at 28°C, and with an initial pH of 7.5. To investigate the effect of salinity on crystallization, bacterial strains were inoculated in TSB media with 2.0%, 4.0%, 6.0%, and 8.0% sea salt. For structural and element content analysis, mineral crystals were isolated from TSA agar medium supplemented with 3.0% sea salt, because of a higher yield in such a condition. The mineral crystals were formed in the agar medium or on the surface. Potassium iodide (KI) was used as the chaotropic salt that conforms to the Hofmeister series (Saito, 1969; Zhang and Cremer, 2006). The TSA medium was cut into cubes and placed into 100 mL of pure water before KI was added. When heated at 70°C for half an hour, the mineral crystals were seen to precipitate from the agar. We also added 200 μL of ammonia solution of analytical grade (Jiuyi, Shanghai, China) to 39.8 mL of TSB medium supplemented with 3.0% sea salt, and no bacterial incubation to induce mineral crystal as a control, in which the final ammonia concentration measured was 572.7 mg/L. This concentration was of a similar level to that of the 2216E medium after 6 days' incubation. A commercial struvite ($NH_4MgPO_4{\cdot}6H_2O$) (Macklin, Shanghai, China) was used as standard for the identification of mineral crystals induced by bacterial strains.

2.5 Mineral crystal characterization

Scanning electron microscopy–energy-dispersive spectrometry (SEM-EDS; FEI, USA) using double-beam scanning was used to detect the difference in elemental composition between mineral crystals induced by bacterial strains, mineral crystals produced by adding ammonia to TSB medium, and commercial struvite. Fourier-transform infrared microscopy (FTIR; IS50, Thermo Fisher Scientific Inc., USA) was performed in a scanning range of 400–4,000 cm^{-1}, with the potassium bromide technique used to detect the surface functional groups of the mineral crystal. The scanning angle (2θ) of the X-ray diffractometer (XRD; D8 Advance, Brucker, Germany) ranged from 10° to 90°, with a step size of 0.02° and a count time of 8° min^{-1}. Data from the XRD were analyzed by Jade (v6.5) software (Mechanical Dynamics, Inc., USA) to determine the composition of mineral crystal induced by bacterial strains. A comparison was made with the experimental diffraction data of struvite standard in the powder diffraction file (PDF) of the International Center for Diffraction Data (ICDD) to confirm whether or not the mineral crystal was struvite mineral. Thermogravimetric (TG) analysis, differential thermal gravity (DTG), and differential scanning calorimetry (DSC) analysis were conducted with a simultaneous thermal analyzer (STA 449F3, Netzsch, Germany) in a temperature range of 29–1,000°C at a heating rate of 10°C/min to assess the thermal stability and composition of the mineral crystal.

2.6 Genetic analysis of ammonia-producing metabolic pathways

To determine pathways involved in producing ammonia among the genus *Alteromonas*, gene families of ammonification, which includes glutamate dehydrogenation (*gdh_K00260*, *gdh_K00261*, *gdh_K00262*, and *gdh_K15371*), assimilatory nitrate reduction (*nasA*, *nasB*, *nirA*, *NR*, *narB*, and *narC*), and dissimilatory nitrate reduction (*napA*, *NapA*, *napB*, *napC*, *narG*, *narH*, *narJ*, *narI*, *narZ*, *nary*, *narV*, *narW*, *nirB*, *nirD*, *nrfA*, *nrfB*, *nrfC*, and *nrfD*), were extracted from the NCycDB database (Tu et al., 2019). Sequences of each gene family were sorted by length, the longest quarter and shortest quarter were removed, and the remaining half was used to build profile hidden Markov models (HMMs) using the program hmmbuild in the HMMER package, version 3.0 (http://hmmer.org). The program hmmsearch in HMMER was used for homolog identification of ammonification genes against genomes of the genus *Alteromonas* with an E-value cut-off point of 1e-10. All the candidate genes were further submitted to the online annotation tool BlastKOALA (https://www.kegg.jp/blastkoala/) (Kanehisa et al., 2016) to verify whether or not they were a member of related gene family. All the genomes of the genus *Alteromonas* available in the RefSeq database on NCBI (National Center for Biotechnology Information) were downloaded and subjected to ammonification gene analysis. The bac120 gene set was used to build a genome-based phylogenetic tree with EasyCGTree, version 4.0 (https://github.com/zdf1987/EasyCGTree4) (Xue et al., 2021).

3 Results

3.1 *Alteromonas* spp. can induce mineral crystals in either agar or broth media with different sea salt concentrations

After incubation for 7 days at 28°C on TSA plates, mineral crystals induced by the five *Alteromonas* strains were visible to the naked eye. The crystals had radial or acicular forms and were of different sizes (Figure 1). The crystals produced by *A. alteriprofundi* HHU 13199^T and *A. lutimaris* KCTC 23464^T had smaller sizes, of < 3 mm, whereas those of *A. chungwhensis* KCTC 12239^T had larger sizes, of about 1 cm. Subsequently, *A. alteriprofundi* HHU 13199^T and *A. alterisediminis* N102^T were selected as representatives to analyze the effect of different sea salt concentrations on mineral crystallization for their apparent divergence among the five strains (Zhang et al., 2021). Mineral crystals were induced in the TSB medium with different sea salt concentrations (2%, 4%, 6%, and 8%) after about 10 days of incubation (Figure 2). The results of scanning electron microscopy (SEM) suggested that the size and morphology of the mineral crystal particles did not change significantly as the sea salt concentrations increased. The crystals were approximately 200–300 μm in size and relatively regular in shape, with several crystals coalescing at low concentrations (Figure 2). With higher sea salt concentrations, there was a greater tendency to form individual, elongated crystals in strips, and the surface of all crystals was relatively smooth. The crystals induced in the TSB media were found to be not as large in size as those observed in TSA media; the reason for this may be that the large crystals were broken down during culturing vibration and sample collection.

3.2 *Alteromonas* spp. induce mineral crystals by ammonification

During induction experiments of mineral crystal formation in 2216E medium, we noticed that the pH increased to > 8.0 after incubation. Therefore, it is hypothesized that the production of ammonia contributes to an increase in pH. Strains *A. alteriprofundi* HHU 13199^T and *A. alterisediminis* N102^T were incubated in 2216E broth to monitor ammonia content during culture. The results (Figure 3A) show that the pH of the 2216E medium increased from 7.5 to 8.6 after 5 days of incubation for both strains, and that the increase in pH may have provided an alkaline environment that favored the formation of struvite. The initial NH_3-N concentration was approximately 20.3 mg/L, increasing to approximately 606.7 mg/L after 5 days (Figure 3B). The increased NH_3-N content in the medium also contributed toward the alkaline environment. The NO_3-N content decreased from an initial level of approximately 130–150 mg/L to approximately 10–30 mg/L (Figure 3C). This indicates that *A. alteriprofundi* HHU 13199^T and *A. alterisediminis* N102^T both have the ability to produce ammonia by nitrate reduction and to cause a pH increase in the environment.

3.3 Characterization of mineral crystals

Strains *A. alteriprofundi* HHU 13199^T and *A. alterisediminis* N102^T were grown on TSA medium to collect mineral crystals for further characterization because of the higher yields of crystals obtained when the strains were grown in this medium. SEM-EDS was used to determine the morphology and elemental composition of the mineral crystals. SEM results showed that mineral crystals induced by *A. alteriprofundi* HHU 13199^T (Figures 4A, B) mainly had a thin columnar form. Mineral crystals induced by *A. alterisediminis* N102^T were also mainly of thin columnar form, with some irregular forms (Figures 4D, E). Mineral crystals produced by adding ammonia to TSB medium were regular and blocky in shape (Figures 4G, H). Commercial struvite crystals were blocky and had a thin columnar form (Figures 4J, K). The mineral particles mentioned above varied in size on the micro-scale. EDS results showed that the elemental composition of mineral crystals induced by *A. alteriprofundi* HHU 13199^T and *A. alterisediminis* N102^T was C, O, Na, Mg, P, K, and Ca (Figures 4C, F). The mineral crystals produced by adding ammonia to the TSB medium had an elemental composition of O, Na, Mg, P, K, and Ca (Figure 4I).

XRD was used to confirm the crystal phase and the structure of the mineral crystals induced by *A. alteriprofundi* HHU 13199^T and *A. alterisediminis* N102^T. The results (Figure 5Aa) implied that the diffraction peaks (2θ) of mineral crystals induced by *A. alteriprofundi* HHU 13199^T at 15.226, 15.960, 16.695, 21.063, 21.676, 25.207, 27.289, 30.270, 30.759, and 33.413 were relevant to the Miller (hkl)

10.3389/fmars.2023.1085345

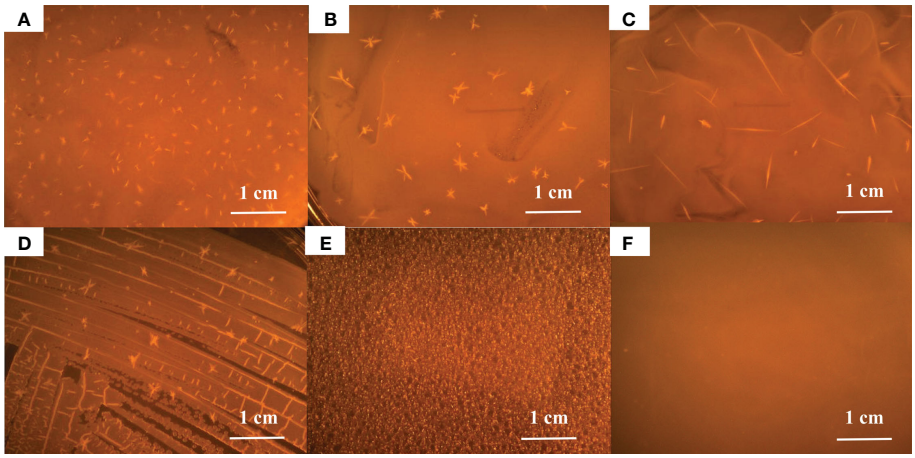

FIGURE 1
Mineral crystals induced by *Alteromonas* on TSA+2.5% sea salt. **(A)**, *A. alteriprofundi* HHU 13199^T; **(B)**, *A. alterisediminis* N102^T; **(C)**, *A. chungwhensis* KCTC 12239^T; **(D)**, *A. iocasae* MCCC 1K03884^T; **(E)**, *A. lutimaris* KCTC 23464^T; **(F)**, control.

indices (110), (020), (011), (111), (021), (121), (130), (012), (211), and (022), respectively. The interplanar crystal spacing values (d) corresponding to the diffraction peaks (2θ) were 5.8141, 5.5484, 5.3058, 4.2144, 4.0967, 3.5301, 3.2653, 2.9502, 2.9044, and 2.6795, respectively. The diffraction peaks (2θ) of mineral crystals induced by *A. alterisediminis* N102^T (Figure 5Ab) at 15.266, 16.062, 16.756, 21.104, 21.716, 30.453, 30.820, 33.943, 38.577, and 46.599 were relevant to the (hkl) indices (110), (020), (011), (111), (021), (012), (211), (221), (231), and (103), respectively. The interplanar crystal spacing values (d) corresponding to the diffraction peaks (2θ) were 5.7991, 5.5133, 5.2866, 4.2062, 4.0890, 2.9329, 2.8988, 2.6389, 2.3319, and 1.9474, respectively. The diffraction peaks (2θ) of mineral crystals produced by adding ammonia to the TSB medium (Figure 5Ac) at 15.205, 16.000, 16.613, 21.043, 21.655, 25.840, 27.248, 29.718, 30.292, 30.799, 32.107, 33.331, 33.862, 38.455, 45.130, and 46.518 were relevant to the (hkl) indices (110), (020), (011), (111), (021), (200), (130), (201), (012), (211), (040), (022), (221), (231), (151), and (103), respectively. The interplanar crystal spacing values (d) corresponding to the diffraction peaks (2θ) were 5.8221, 5.5348, 5.3317, 4.2183, 4.1005, 3.4450, 3.2701, 3.0037, 2.9386, 2.9026, 2.7856, 2.6858, 2.6450, 2.3390, 2.0074, and 1.9507, respectively. The diffraction peaks (2θ) of the commercial struvite ($NH_4MgPO_4{\cdot}6H_2O$) (Figure 5Ad) at 15.144, 15.960, 16.614, 21.002, 21.614, 25.779, 27.228, 29.678, 30.351, 30.759, 32.066, 33.413, 33.801, 38.414, 45.068, and 46.457 were relevant to the (hkl) indices (110), (020), (011), (111), (021), (200), (130), (201), (012), (211), (040), (022), (221), (231), (151), and (103), respectively. The interplanar crystal spacing values (d) corresponding to the diffraction peaks (2θ) were 5.8462, 5.5491, 5.3316, 4.2267, 4.1081, 3.4532, 3.0079, 2.9423, 2.9044, 2.7890, 2.6795, 2.6496, 2.3414, 2.0099, and 1.9530, respectively. The mineral crystals induced by the bacterial strains and the ammonia-added sample were compared with the PDF of the struvite mineral (no. 15-0762).

To determine the group composition of mineral crystals induced by bacterial strains and in the ammonia-added sample, FTIR analysis was carried out. The results (Figure 5B) indicate that absorption peaks at 2,910, 2,880, and 2,360 cm^{-1} are in the vibration peaks of the symmetric stretching vibration and unsymmetrical stretching vibration of the hydrogen bond (O-H) of water (Sinha et al., 2014) and the N-H in the NH_4^+ group. The peaks at 1,430 cm^{-1} arise from the unsymmetrical bending vibration of the N-H (NH_4^+) (Korchef et al., 2011; Moulessehoul et al., 2017; Manzoor et al., 2019; Guan et al., 2021). The peaks at 979, 980, 987, 989, 563, 564, 565, 460, 461, and 462 cm^{-1} are the vibration peaks of the phosphoric acid group. The peaks at 746, 747, 748, and 751 cm^{-1} are assigned to the vibration of the hydrogen bonds among the water molecules.

The TG–DTG–DSC results (Figure 6A) imply that thermal weight loss of mineral crystal induced by *A. alteriprofundi* HHU 13199^T was mainly divided into two stages: the first stage was from 29°C to 146.93°C, accounting for 33.83% of the total weight; and the second stage was from 146.93°C to 1,000°C, accounting for 17.97% of the total weight. The results (Figure 6B) show that the thermal weight loss of the mineral crystal induced by *A. alterisediminis* N102^T was also divided into two stages: the first stage was from 29°C to 148.98°C, accounting for 36.03% of the total weight; and the second stage was from 148.98°C to 1,000°C, accounting for 16.39% of the total weight. The first stages of struvite formation induced by strains were mainly caused by the loss of crystalline water, and the second stages were attributed to the instability of ammonium and decomposition of ammonium to ammonia. Commercial struvite mineral ($NH_4MgPO_4{\cdot}6H_2O$) (Figure 6D), struvite mineral obtained in TSB medium with ammonia (Figure 6C), and struvite mineral induced by bacterial strains in the TSA medium (Figures 6A, B) all had two weight loss stages, which were caused by the loss of crystal water and the instability of ammonium and decomposition of ammonium to ammonia, respectively. The thermal stability was similar between mineral crystals induced by the bacterial strains, mineral crystals produced by the ammonia-added sample and commercial struvite mineral.

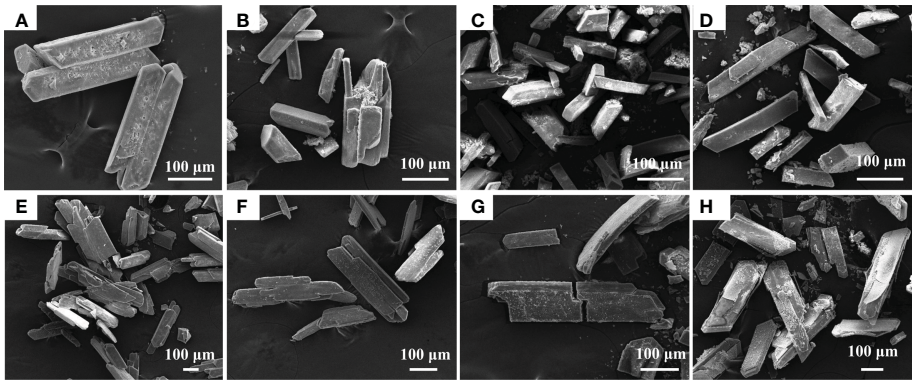

FIGURE 2
Scanning electron microscope (SEM) analysis of mineral crystals induced by *Alteromonas* at different concentrations of sea salt. *Alteromonas* spp. were cultured in TSB supplemented with different sea salt concentrations (2%, 4%, 6%, 8%, from left to right) for 5 days. **(A–D)**, *A. alteriprofundi* HHU 13199^T; **(E–H)**, *A. alterisediminis* N102^T.

3.4 Ca^{2+} and/or Mg^{2+} can promote growth of *Alteromonas* spp.

By gradually reducing the components in seawater (Table S2), it was found that *A. alteriprofundi* HHU 13199^T could grow on media TSA I and TSA II, which contained Mg^{2+} and Ca^{2+}, respectively, but no growth occurred on media TSA III and TSA IV. Subsequently, *A. alteriprofundi* HHU 13199^T and *A. alterisediminis* N102^T were cultured in TSB media supplemented with NaCl and different concentrations of eight Mg^{2+} or Ca^{2+}, respectively.

Both Ca^{2+} and Mg^{2+} had a growth-stimulating effect on both strains of the genus *Alteromonas* (Figure 7, Table S3). However, different concentrations of Ca^{2+} and Mg^{2+} had different stimulating effects on the growth of the strains. When $CaCl_2$ was added at a concentration less than 0.414 g/L (0.3×, ≈ 3.6 mM Ca^{2+}), growth of *A. alteriprofundi* HHU 13199^T (Figure 7A) and *A. alterisediminis*

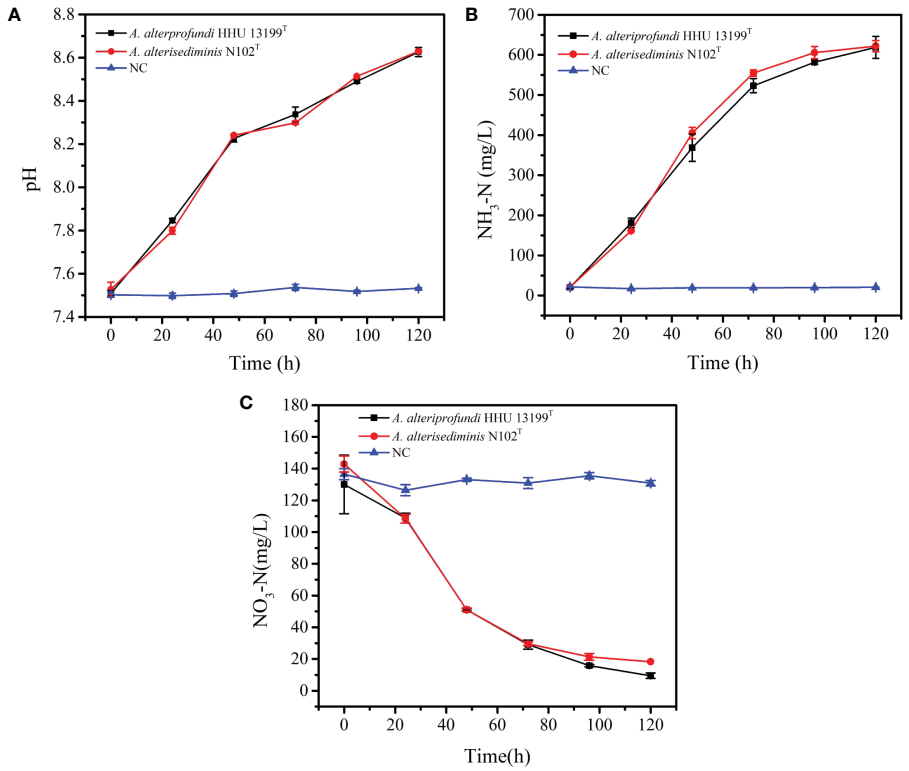

FIGURE 3
Changes in pH value, NH_3-N, and NO_3-N concentration in 2216E medium during the incubation of strains *A. alteriprofundi* HHU 13199^T and *A. alterisediminis* N102^T. **(A)**, pH value; **(B)**, NH_3-N concentration; **(C)**, NO_3-N concentration.

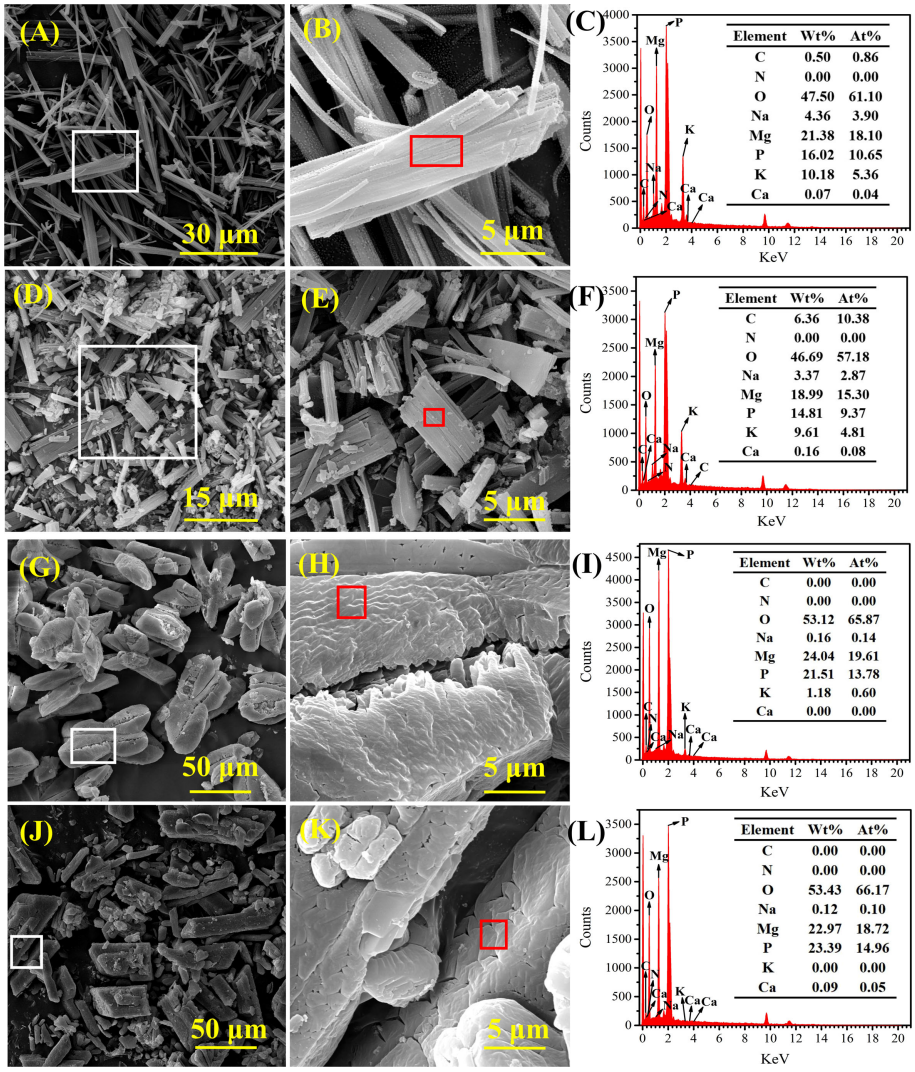

FIGURE 4
Scanning electron microscope (SEM) and energy dispersive spectrum (EDS) images of mineral crystals induced by strains *A. alteriprofundi* HHU 13199^T **(A–C)**, *A. alterisediminis* N102^T **(D–F)**, ammonia solution **(G–I)**, and commercial struvite standard ($NH_4MgPO_4{\cdot}6H_2O$) **(J–L)**, respectively.

N102^T (Figure 7B) was suppressed (generation time > 50 h; Table S3). When $MgCl_2{\cdot}6H_2O/MgSO_4{\cdot}7H_2O$ was added at a concentration less than 0.2× (9.50 mM Mg^{2+}) and 0.1× (4.75 mM Mg^{2+}), growth of *A. alteriprofundi* HHU 13199^T (Figure 7D) and *A. alterisediminis* N102^T (Figure 7D) was suppressed, respectively (generation time > 50 h; Table S3). When higher concentrations (especially >0.7×) of Ca^{2+} or Mg^{2+} were added, the growth rate and the final biomass tended to reach a steady state. These results suggest that the Ca^{2+} and Mg^{2+} contents in normal Backhaus ASW were very close to the optimal concentration required for the growth of both strains. In addition, *A. alteriprofundi* HHU 13199^T needed higher Ca^{2+} and/or Mg^{2+} content to start reproducing, which implied a dependence on Ca^{2+} and/or Mg^{2+} for its growth.

3.5 Pathways of ammonification metabolism are commonly present in the genus *Alteromonas*

In total, 126 genomes of the genus *Alteromonas* were retrieved from the RefSeq database, comprising 82 strains from 32 known species and 44 unclassified isolates (Figure 8). All the strains were found to be harboring at least three genes related to ammonification metabolism, and 10 genes were detected in the genus *Alteromonas*. For gene-encoding glutamate dehydrogenase, homologs of *gdh_K00262* and *gdh_K15371* were found in 99 (78.6%) and 125 (99.2%) genomes, respectively. For genes conferring dissimilatory nitrate reduction, *narG*, *narH*, and *narI* were detected in five (4.0%), four (3.2%), and five (4.0%) genomes, respectively. For genes

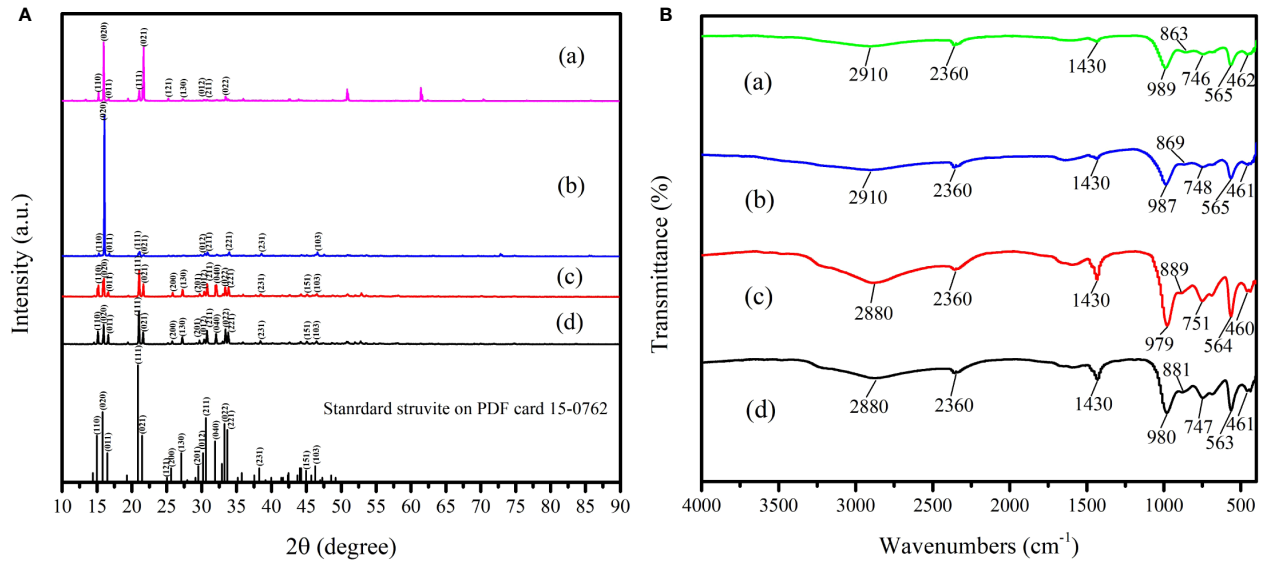

FIGURE 5
X-ray diffraction (XRD, **A**) and Fourier-transform infrared microscopy (FTIR, **B**) analysis of mineral crystals induced by bacterial strains in TSA medium, and ammonia solution in TSB medium. (a), the mineral crystals obtained in TSA medium with *A. alteriprofundi* HHU 13199^{T}; (b), the mineral crystals obtained in TSA medium with *A. alterisediminis* N102^{T}; (c), the mineral crystals obtained in TSB medium with ammonia; (d), the commercial struvite standard. Black bars show the struvite standard in PDF no. 15-0762.

conferring dissimilatory nitrite reduction, *nirB* and *nirD* were detected in 113 (89.7%) and 114 (90.5%) genomes, respectively. For genes conferring assimilatory nitrate reduction, *nasA* and *narW*/*narJ* were detected in 111 (88.1%) and five (4.0%) genomes, respectively. For genes conferring assimilatory nitrite reduction, *nirA* was detected in 124 (98.4%) genomes. *A. chungwhensis* KCTC 12239^{T}, *A. iocasae* MCCC 1K03884^{T}, *A. lutimaris* KCTC 23464^{T}, and *A. alteriprofundi* HHU 13199^{T}

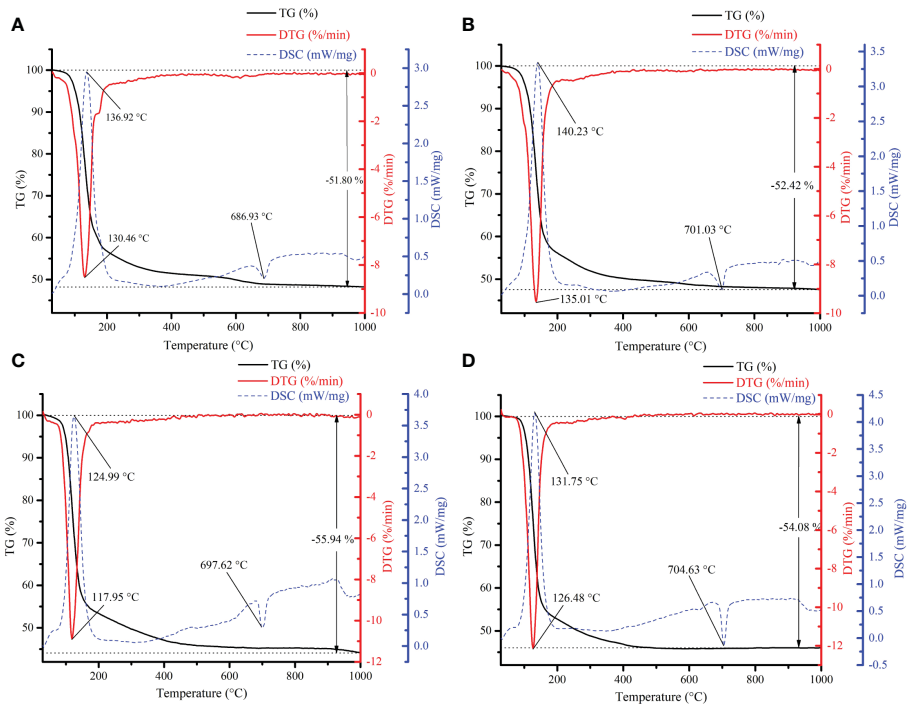

FIGURE 6
Thermogravimetric, differential thermal gravity and differential scanning calorimetry (TG–DTG) analysis of mineral crystals. **(A)**, the mineral crystals induced by *A. alteriprofundi* HHU 13199^{T} in TSA medium; **(B)**, the mineral crystals induced by *A. alterisediminis* N102^{T} in TSA medium; **(C)**, the struvite obtained in TSB medium with ammonia; **(D)**, the commercial struvite standard.

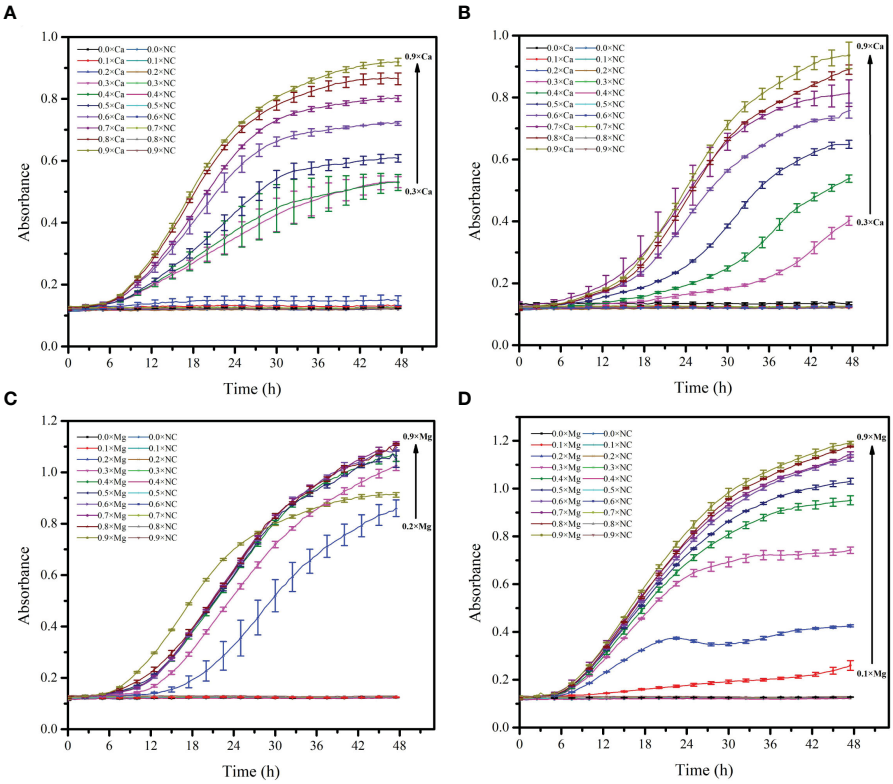

FIGURE 7
Growth curve of *Alteromonas* with different concentrations of Ca^{2+} and Mg^{2+}. **(A, C)**, *A. alteriprofundi* HHU 13199^{T}; **(B, D)**, *A. alterisediminis* N102^{T}.

harbored *gdh_K00262* and *gdh_K15371*, and *nirA*, whereas *A. alterisediminis* N102^{T} harbored *nirB* and *nirD*. These five strains had fewer genes detected to be associated with ammonification metabolism among the genus *Alteromonas*. In contrast, three species, *A. alba* (GCF 002993365.1), *A. mediterranea* (GCF 927797765.1), and unclassified *Alteromonas* sp. (GCF 020515205.1), were found to be harboring 10 genes related to ammonification metabolism. Gene content identical to *A. alterisediminis* N102^{T} was also identified in *A. macleodii* (GCF 000299995.1), whereas gene content identical to the other four strains was also found in *A. sediminis* (GCF 003820355.1), *A. ponticola* (GCF 012911815.1), *A. halophila* (GCF 014651815.1), *Salinimonas marina* (GCF 015644725.1), *A. hispanica* (GCF 010500915.1), and *Alteromonas* sp. (GCF 000753915.1 and GCF 000753865.1).

4 Discussion

The phenomenon of bacterial biomineralization has long been recognized, and a variety of minerals have been reported to be induced by species of bacteria (Beveridge, 1989; Gonzalez-Munoz et al., 2012; Diaz et al., 2017; Vigliaturo et al., 2020). For example, *Bacillus licheniformis* can induce calcite, vaterite, monohydrocalcite, and nesquehonite to remove calcium and magnesium from the environment by desalination (Zhao et al., 2019). *Leclercia adecarboxylata* JLS1 and *Enterobacter* sp. EMB19 can enrich phosphorus in the environment and mineralize to form struvite (Sinha et al., 2014; Han et al., 2017). *Citrobacter freundii* isolated from marine sediments can be used to induce the precipitation of carbonate and phosphate minerals under anaerobic conditions (Sun et al., 2020). However, reports focusing on biomineralization of marine bacteria are rare, in spite of the fact that precipitation of barite and calcite by marine bacteria have been documented (Gonzalez-Munoz et al., 2012; Sullivan and Murdaugh, 2014; Torres-Crespo et al., 2015; Wei et al., 2015; Sarayu et al., 2016; Yasumoto-Hirose et al., 2022). In this study, we found that five *Alteromonas* spp. from marine environments possess the ability to induce mineral crystals with special morphology in both agar and broth media. These results broadened the range of bacterial taxa that are responsible for mineral production.

In this study, it was observed that bacterial strains induced more struvite crystals in TSA medium than in 2216E medium, but the exact number and size differences were not recorded. It is thought that one of the reasons for this is that TSA medium (Bacto^{TM}) is eutrophic, with more nutrients, such as peptide/protein and phosphate, than 2216E medium, which facilitates bacterial induction of struvite crystal production. All five *Alteromonas* spp. induced mineral crystal formation in TSA agar medium that was supplemented with 2.5% sea salt. The strain *A. lutimaris* KCTC 23464^{T} formed hard biofilms on the medium surface, and mineral crystals were formed in both the biofilm and the medium (Figure 1E). This is different from the other four strains. The mineral crystals formed by the different *Alteromonas* spp. showed

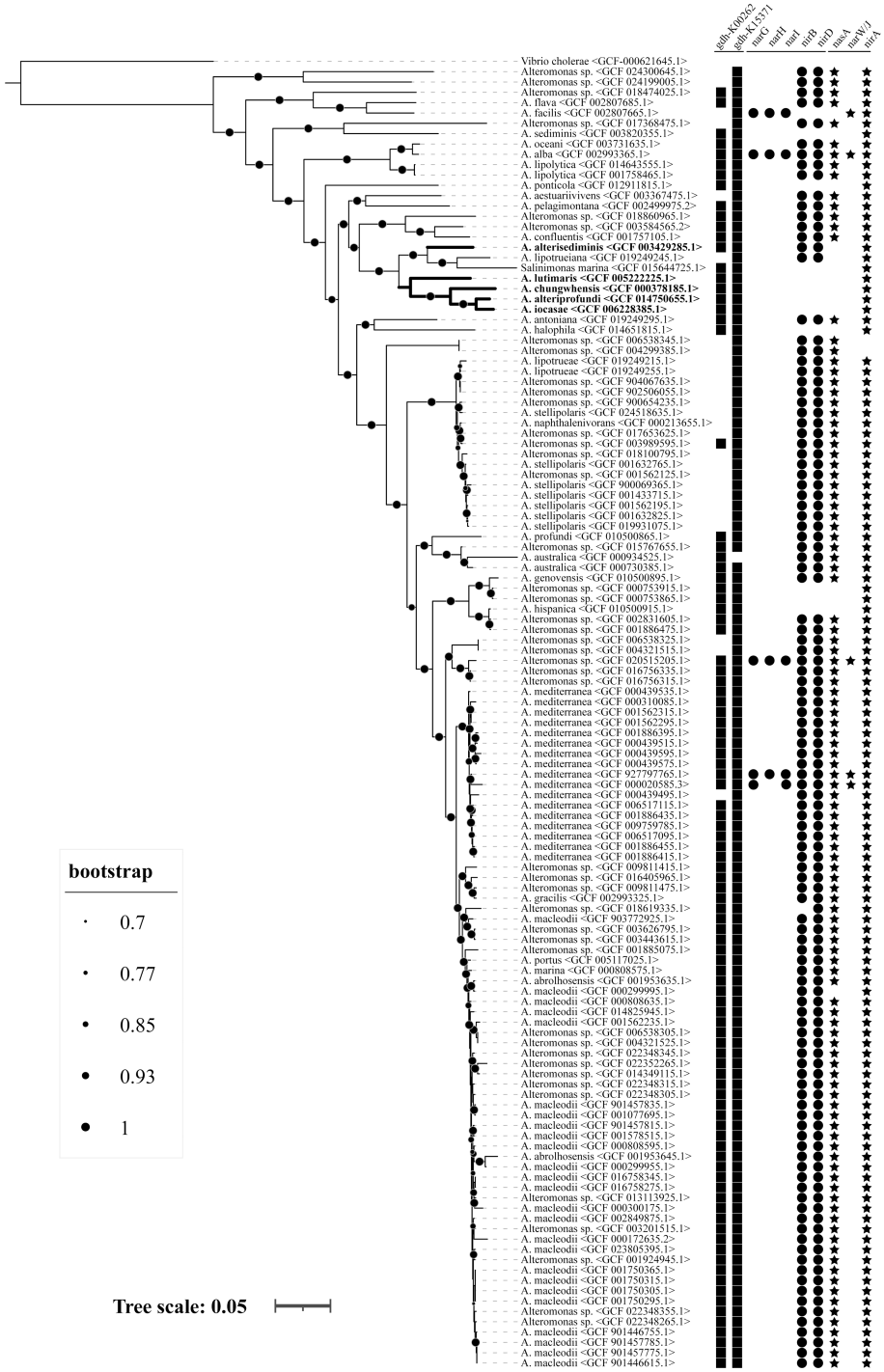

FIGURE 8
Genome-based phylogenetic tree and prevalence of ammonia-producing metabolic pathway in the genus *Alteromonas*. A total of 126 genomes, comprising 82 strains from 32 known species and 44 unclassified isolates, were used for analysis. Different sizes of dots on the branch represent different bootstrap values. Squares represent genes *gdh_K00262* and *gdh_K15371*; dots represent genes *narD*, *narH*, *narI*, *nirB*, and *nirD*; stars represent genes *nasA*, *narW/J*, and *nirA*, respectively.

differences in shape, and it can be deduced that the morphology of the mineral crystals is influenced by the strains themselves. Because strains *A. alteriprofundi* HHU 13199^T and *A. alterisediminis* N102^T were the furthest apart in the evolutionary tree, with the other three strains more closely related (Figure 8), the results from these two strains were taken to be representative of the mineral crystals induced by *Alteromonas* spp. in this study. SEM results showed that there was no significant change in the size and morphology of the mineral crystals induced by either strain when increasing the sea salt concentrations, indicating that the sea salt concentration had limited influence on the morphology of the mineral crystals. FTIR results showed that mineral crystals induced by bacterial strains and

TABLE 1 The cell parameter of mineral crystals analyzed by Jade (v6.5).

Cell parameter	a (nm)	b (nm)	c (nm)	V (A^3)	Density
1	6.90564	11.06721	6.09239	465.62	1.7503
2	6.91318	11.02619	6.09424	464.54	1.7543
3	6.89722	11.13713	6.12175	470.24	1.7330
4	6.91546	11.1517	6.10595	470.89	1.7307
5	6.94510	11.2080	6.13550	477.58	1.7064

a, b, and c represent the edge length of the crystal. (1) A. alteriprofundi HHU 13199^T; (2) A. alterisediminis N102^T; (3) the mineral crystals obtained in TSA medium with ammonia; (4) the commercial struvite standard ($NH_4MgPO_4{\cdot}6H_2O$); and (5) the struvite standard in PDF no. 15-0762.

the ammonia-added sample all included the characteristic absorption bands of crystalline water, NH_4^+, and PO_4^+, may be struvite mineral (Han et al., 2015). SEM–EDS results indicated that mineral crystals induced by bacterial strains and the ammonia-added sample both had the elements O, Mg, P, K, Ca, and Na. Among them, O, Mg, and P are the base components of struvite mineral (Figure 4), and C, Na, K, and Ca may come from organic matter metabolized by strains (Wang et al., 2022). The XRD results showed that mineral crystals induced by bacterial strains had the strongest diffraction peak intensity in the crystal plane (020), indicating that mineral crystals mainly grow along the crystal plane (020), whereas mineral crystals of the ammonia-added sample and the standard struvite mineral of the PDF (no. 15-0762) mainly grow along the crystal plane (011). According to the results (Table 1) of the cell parameters analyzed with Jade (v6.5), both mineral crystals induced by bacterial strains and the ammonia-added sample were more compact than the commercial struvite, but mineral crystals induced by bacterial strains were more compact than those induced by the ammonia-added sample. All mineral crystal samples had similar interplanar spacing. This shows that the growth direction of mineral crystals produced by *A. alteriprofundi* HHU 13199^T and *A. alterisediminis* N102^T was the same, but different from that of the ammonia-added sample and the standard struvite crystals. This can be used to support the hypothesis that bacteria and their metabolites can influence nucleation and crystal growth (Han et al., 2017). The results of SEM–EDS and XRD proved that mineral crystals induced by the bacterial strains and the ammonia-added sample were struvite mineral when compared with the standard struvite mineral in the PDF (no. 15-0762).

The formation of struvite induced by bacteria was first reported in 1889 (Han et al., 2015), and, to date, many microorganisms have been reported to possess the ability to induce the formation of struvite, including *Acinetobacter calcoaceticus*, *Azotobacter*, *Bacillus pumilus*, *Brevibacterium antiquum*, *Brucella*, *Corynebacterium*, *Enterobacter*, *Flavobacterium*, *Halobacterium salinarumand*, *Idiomarina loihiensis*, *Myxococcus xanthus*, *Proteus mirabilis*, *Pseudomonas*, *Shewanella oneidensis*, and *Ureaplasma urealyticum* (Da Silva et al., 2000; Sun et al., 2012; Sinha et al., 2014; Han et al., 2015; Han et al., 2017; Manzoor et al., 2018; Leng and Soares, 2021; Zhang et al., 2022). However, to our knowledge, there are few marine bacteria that have been reported to be responsible for the formation of struvite. As mentioned above, the genus *Alteromonas* comprises versatile microorganisms playing essential roles in marine biogeochemical cycles (Lelchat et al., 2015; Chen et al., 2020; Cusick et al., 2021; Gago et al., 2021). In this study, we suggest that *Alteromonas* spp. can induce struvite formation under various laboratory conditions (Figure 1), which sheds new light on the ecological roles of these bacteria in marine environments. Furthermore, *A. alteriprofundi* HHU 13199^T and *A. alterisediminis* N102^T were taken as representative and their growth was determined with the dependence on Ca^{2+} and/or Mg^{2+} content. Surprisingly, the optimal concentration of Ca^{2+} and Mg^{2+} was very close to that in normal sea water (Figure 7), which further proved that *Alteromonas* spp. are indigenous to marine environments.

The formation of minerals in environments is very closely associated with the physiological and biochemical activities of microorganisms, and it was believed that struvite could be induced by microbes when the correct quantities of magnesium, ammonium, and phosphate were present (Rivadeneiea et al., 1985; Ronholm et al., 2014; Han et al., 2015; Han et al., 2017). In this study, struvite induced by *Alteromonas* spp. and ammonium solution were determined to have similar traits (Figure 4), which implied that *Alteromonas* spp. induced struvite by releasing ammonium to raise the environmental pH and provided NH_4^+ for the formation of struvite. Together with the observation that the struvite was mainly formed in the agar media and rarely linked to bacterial mass, the related mechanism of *Alteromonas* spp. could be categorized as BIM, according to previous descriptions (Frankel and Bazylinski, 2003; Park and Faivre, 2022). The monitoring of NH-N and NO_3-N content changes in the liquid culture of *Alteromonas* spp. also provided evidence for this conjecture (Figure 3). Further genetic analysis showed that pathways of ammonification metabolism were universally present in the genus *Alteromonas* (Figure 8). The five *Alteromonas* spp. that could produce ammonium and induce struvite possessed fewer genes involved in ammonification metabolism. In particular, genes conferring assimilatory or dissimilatory nitrate reduction were not detected except in *A. alterisediminis*. These results suggest that these bacteria probably harbor novel gene(s) to accomplish the function of nitrate reduction. In addition, these results imply that other bacteria of the genus *Alteromonas* with gene content identical to *A. alterisediminis* N102^T or the other four strains used in this study could perform a biomineralization function.

5 Conclusion

In summary, we suggested that five *Alteromonas* spp. can induce mineral crystallization in laboratory conditions, and further characterized the mineral crystals induced by *A. alteriprofundi* HHU 13199^T and *A. alterisediminis* N102^T as struvite. The related mechanism was categorized as BIM, with ammonium release causing pH increase by the strains during growth through nitrate reduction. Nevertheless, some genes essential to conferring the function of nitrate reduction to ammonium were identified to be absent in four of the five strains used to induce mineral crystals. These results implied that there may be a novel gene family present in these strains, which should be clarified in the future. Prevalence analysis of ammonification metabolism pathways suggested that ammonium production was ubiquitous among the genus *Alteromonas*. Considering *Alteromonas* is indigenous in marine environments and has adapted to high salinity (Ivars-Martinez et al., 2008; Gonzaga et al., 2012; Chen et al., 2020; Gago et al., 2021), it is reasonable to question the role of *Alteromonas* spp. in struvite deposition in the ocean and sea. This will lead to a clearer picture of the role that the genus *Alteromonas* plays in marine geochemical circulation.

Data availability statement

The datasets presented in this study can be found in online repositories. The names of the repository/repositories and accession number(s) can be found in the article/Supplementary Material.

Author contributions

WH: data curation, formal analysis, investigation, visualization, and writing—original draft. H-PX: methodology, data curation, formal analysis, and investigation. CL: methodology, data curation, formal analysis, writing—review, and editing. AZ: methodology, resources, and formal analysis. J-KH: writing—review and editing. D-FZ: conceptualization, methodology, project administration, writing—review and editing, and funding acquisition. All authors contributed to the article and approved the submitted version.

Funding

The study was supported by the National Natural Science Foundation of China (No. 31900001), and the Fundamental Research Funds for the Central Universities (B210202140).

Conflict of interest

The authors declare that the research was conducted in the absence of any commercial or financial relationships that could be construed as a potential conflict of interest.

Publisher's note

All claims expressed in this article are solely those of the authors and do not necessarily represent those of their affiliated organizations, or those of the publisher, the editors and the reviewers. Any product that may be evaluated in this article, or claim that may be made by its manufacturer, is not guaranteed or endorsed by the publisher.

Supplementary material

The Supplementary Material for this article can be found online at: https://www.frontiersin.org/articles/10.3389/fmars.2023.1085345/full#supplementary-material

References

Beam, J. P., Scott, J. J., McAllister, S. M., Chan, C. S., McManus, J., Meysman, F. J. R., et al. (2018). Biological rejuvenation of iron oxides in bioturbated marine sediments. *ISME J.* 12 (5), 1389–1394. doi: 10.1038/s41396-017-0032-6

Beveridge, T. J. (1989). Role of cellular design in bacterial metal accumulation and mineralization. *Annu. Rev. Microbiol.* 43, 147–171. doi: 10.1146/annurev.mi.43.100189.001051

Bruins, M. R., Kapil, S., and Oehme, F. W. (2000). Microbial resistance to metals in the environment. *Ecotox. Environ. Safe.* 45 (3), 198–207. doi: 10.1006/eesa.1999.1860

Cao, J., Lai, Q., Liu, P., Wei, Y., Wang, L., Liu, R., et al. (2018). *Salinimonas sediminis* sp. nov., a piezophilic bacterium isolated from a deep-sea sediment sample from the new Britain trench. *Int. J. Syst. Evol. Microbiol.* 68 (12), 3766–3771. doi: 10.1099/ijsem.0.003055

Chen, M., Song, Y., Feng, X., Tang, K., Jiao, N., Tian, J., et al. (2020). Genomic characteristics and potential metabolic adaptations of hadal trench *Roseobacter* and *Alteromonas* bacteria based on single-cell genomics analyses. *Front. Microbiol.* 11. doi: 10.3389/fmicb.2020.01739

Cusick, K., Iturbide, A., Gautam, P., Price, A., Polson, S., MacDonald, M., et al. (2021). Enhanced copper-resistance gene repertoire in *Alteromonas macleodii* strains isolated from copper-treated marine coatings. *PloS One.* 16 (9), e0257800. doi: 10.1371/journal.pone.0257800

Da Silva, S., Bernet, N., Delgenes, J. P., and Moletta, R. (2000). Effect of culture conditions on the formation of struvite by *Myxococcus xanthus*. *Chemosphere.* 40 (12), 1289–1296. doi: 10.1016/S0045-6535(99)00224-6

Debeljak, P., Toulza, E., Beier, S., Blain, S., and Obernosterer, I. (2019). Microbial iron metabolism as revealed by gene expression profiles in contrasted southern ocean regimes. *Environ. Microbiol.* 21 (7), 2360–2374. doi: 10.1111/1462-2920.14621

Deng, S., Dong, H., Lv, G., Jiang, H., Yu, B., and Bishop, M. E. (2010). Microbial dolomite precipitation using sulfate reducing and halophilic bacteria: Results from qinghai lake, Tibetan plateau, NW China. *Chem. Geology.* 278 (3), 151–159. doi: 10.1016/j.chemgeo.2010.09.008

Diaz, M. R., Eberli, G. P., Blackwelder, P., Phillips, B., and Swart, P. K. (2017). Microbially mediated organomineralization in the formation of ooids. *Geology.* 45 (9), 771–774. doi: 10.1130/G39159.1

Falagán, C., Yusta, I., Sánchez-Espa, A. ,. J., and Johnson, D.B.J.M.E. (2017). Biologically-induced precipitation of aluminium in synthetic acid mine water. *Miner. Eng.* 106, 79–85. doi: 10.1016/j.mineng.2016.09.028

Frankel, R. B., and Bazylinski, D. A. (2003). Biologically induced mineralization by bacteria. *Biomineralization.* 54, 95–114. doi: 10.2113/0540095

Gago, J. F., Viver, T., Urdiain, M., Pastor, S., Kämpfer, P., Ferreira, E., et al. (2021). Description of three new *Alteromonas* species alteromonas antoniana sp. nov., *Alteromonas lipotrueae* sp. nov. and *Alteromonas lipotrueiana* sp. nov. isolated from marine environments, and proposal for reclassification of the genus *Salinimonas* as *Alteromonas*. *Syst. Appl. Microbiol.* 44 (4), 126226. doi: 10.1016/j.syapm.2021.126226

Gao, X., Wen, Y., Qu, D., An, L., Luan, S., Jiang, W., et al. (2018). Interference effect of alcohol on nessler's reagent in photocatalytic nitrogen fixation. *ACS Sustain Chem. Eng.* 6, 5342–5348. doi: 10.1021/acssuschemeng.8b00110

Gonzaga, A., Martin-Cuadrado, A. B., Lopez-Perez, M., Megumi Mizuno, C., Garcia-Heredia, I., Kimes, N. E., et al. (2012). Polyclonality of concurrent natural populations of *Alteromonas macleodii*. *Genome Biol. Evol.* 4 (12), 1360–1374. doi: 10.1093/gbe/evs112

Gonzalez-Munoz, M. T., Martinez-Ruiz, F., Morcillo, F., Martin-Ramos, J. D., and Paytan, A. (2012). Precipitation of barite by marine bacteria: A possible mechanism for marine barite formation. *Geology.* 40 (8), 675–678. doi: 10.1130/G33006.1

Guan, Q., Zeng, G., Song, J., Liu, C., Wang, Z., and Wu, S. (2021). Ultrasonic power combined with seed materials for recovery of phosphorus from swine wastewater *via* struvite crystallization process. *J. Environ. Manage.* 293, 112961. doi: 10.1016/j.jenvman.2021.112961

Han, Z., Sun, B., Zhao, H., Yan, H., Han, M., Zhao, Y., et al. (2017). Isolation of *Leclercia adcarboxglata* strain JLS1 from dolostone sample and characterization of its induced struvite minerals. *Geomicrobiol J.* 34 (6), 500–510. doi: 10.1080/01490451.2016.1222469

Han, Z., Yan, H., Zhao, H., Zhou, S., Han, M., Meng, X., et al. (2014). Bio-precipitation of calcite with preferential orientation induced by *Synechocystis* sp. PCC6803. *Geomicrobiol. J.* 31 (10), 884–899. doi: 10.1080/01490451.2014.907379

Han, Z., Zhao, Y., Yan, H., Zhao, H., Han, M., Sun, B., et al. (2015). Struvite precipitation induced by a novel sulfate-reducing bacterium *Acinetobacter calcoaceticus* SRB4 isolated from river sediment. *Geomicrobiol. J.* 32 (10), 868–877. doi: 10.1080/01490451.2015.1016247

Ivars-Martinez, E., Martin-Cuadrado, A. B., D'Auria, G., Mira, A., Ferriera, S., Johnson, J., et al. (2008). Comparative genomics of two ecotypes of the marine planktonic copiotroph *Alteromonas macleodii* suggests alternative lifestyles associated with different kinds of particulate organic matter. *ISME J.* 2 (12), 1194–1212. doi: 10.1038/ismej.2008.74

Jeon, C. O., Lim, J. M., Park, D. J., and Kim, C. J. (2005). *Salinimonas chungwhensis* gen. nov., sp,, nov., a moderately halophilic bacterium from a solar saltern in Korea. *Int. J. Syst. Evol. Microbiol.* 55, 239–243. doi: 10.1099/ijs.0.63279-0

Kanehisa, M., Sato, Y., Kawashima, M., Furumichi, M., and Tanabe, M. (2016). KEGG as a reference resource for gene and protein annotation. *Nucl. Acids Res.* 44 (D1), D457–D462. doi: 10.1093/nar/gkv1070

Korchef, A., Saidou, H., and Amor, M. B. (2011). Phosphate recovery through struvite precipitation by CO_2 removal: Effect of magnesium, phosphate and ammonium concentrations. *J. Hazard. Mater.* 186 (1), 602–613. doi: 10.1016/j.jhazmat.2010.11.045

Lee, S. H., and Jun, B. H. (2019). Silver nanoparticles: Synthesis and application for nanomedicine. *Int. J. Mol. Sci.* 20 (4), 865. doi: 10.3390/ijms20040865

Lelchat, F., Cozien, J., Le Costaouec, T., Brandilly, C., Schmitt, S., Baudoux, A. C., et al. (2015). Exopolysaccharide biosynthesis and biodegradation by a marine hydrothermal alteromonas sp. strain. *Appl. Microbiol. Biotechnol.* 99 (6), 2637–2647. doi: 10.1007/s00253-014-6075-y

Leng, Y. R., and Soares, A. (2021). The mechanisms of struvite biomineralization in municipal wastewater. *Sci. Total Environ.* 799, 149261. doi: 10.1016/j.scitotenv.2021.149261

Li, F., Jing, X., Zou, C., Zhang, H., and Xiang, F. (2017). Facies analysis of the callovian–oxfordian carbonates in the northeastern amu darya basin, southeastern Turkmenistan. *Mar. Petrol. Geol.* 88, 359–380. doi: 10.1016/j.marpetgeo.2017.08.038

Liu, J. W., Zheng, Y. F., Lin, H. Y., Wang, X. C., Li, M., Liu, Y., et al. (2019). Proliferation of hydrocarbon-degrading microbes at the bottom of the Mariana trench. *Microbiome.* 7, 47. doi: 10.1186/s40168-019-0652-3

Loganathan, P., Naidu, G., and Vigneswaran, S. (2017). Mining valuable minerals from seawater: a critical review. *Environ. Sci.: Water Res. Technol.* 3 (1), 37–53. doi: 10.1039/C6EW00268D

Manck, L. E., Espinoza, J. L., Dupont, C. L., and Barbeau, K. A. (2020). Transcriptomic study of substrate-specific transport mechanisms for iron and carbon in the marine copiotroph *Alteromonas macleodii*. *mSystems.* 5 (2), e00070–20. doi: 10.1128/mSystems.00070-20

Manzoor, M. A. P., Duwal, S. R., Mujeeburahiman, M., and Rekha, P. D. (2018). Vitamin c inhibits crystallization of struvite from artificial urine in the presence of *Pseudomonas aeruginosa*. *Int. Braz. J. Urol.* 44 (6), 1234–1242. doi: 10.1590/S1677-5538.Ibju.2017.0656

Manzoor, M. A. P., Mujeeburahiman, M., Duwal, S. R., and Rekha, P. D. (2019). Investigation on growth and morphology of *in vitro* generated struvite crystals. *Biocatal. Agric. Biotechnol.* 17, 566–570. doi: 10.1016/j.bcab.2019.01.023

McCarren, J., Becker, J. W., Repeta, D. J., Shi, Y., Young, C. R., Malmstrom, R. R., et al. (2010). Microbial community transcriptomes reveal microbes and metabolic pathways associated with dissolved organic matter turnover in the sea. *Proc. Natl. Acad. Sci. U.S.A.* 107 (38), 16420–16427. doi: 10.1073/pnas.1010732107

Moulessehoul, A., Gallart-Mateu, D., Harrache, D., Djaroud, S., de la Guardia, M., and Kameche, M. (2017). Conductimetric study of struvite crystallization in water as a function of pH. *J. Cryst. Growth.* 471, 42–52. doi: 10.1016/j.jcrysgro.2017.05.011

Nayfach, S., Rodriguez-Mueller, B., Garud, N., and Pollard, K. S. (2016). An integrated metagenomics pipeline for strain profiling reveals novel patterns of bacterial transmission and biogeography. *Genome Res.* 26 (11), 1612–1625. doi: 10.1101/gr.201863.115

Nies, D. H. (1999). Microbial heavy-metal resistance. *Appl. Microbiol. Biotechnol.* 51 (6), 730–750. doi: 10.1007/s002530051457

Park, Y., and Faivre, D. (2022). Diversity of microbial metal sulfide biomineralization. *Chempluschem.* 87 (1), e202100457. doi: 10.1002/cplu.202100457

Parte, A. C., Sardà Carbasse, J., Meier-Kolthoff, J. P., Reimer, L. C., and Göker, M. (2020). List of prokaryotic names with standing in nomenclature (LPSN) moves to the DSMZ. *Int. J. Syst. Evol. Microbiol.* 70, 11, 5607–5612. doi: 10.1099/ijsem.0.004332

Pedler, B. E., Aluwihare, L. I., and Azam, F. (2014). Single bacterial strain capable of significant contribution to carbon cycling in the surface ocean. *Proc. Natl. Acad. Sci. U.S.A.* 111 (20), 7202–7207. doi: 10.1073/pnas.1401887111

Purcell, L., and King, A. (1996). Total nitrogen determination in plant material by persulfate digestion. *Agron. J.* 88, 111–113. doi: 10.2134/agronj1996.00021962008800010023x

Rivadeneiea, M. A., Gonzalez-Lopez, J., and Ramos-Cormenzana, A. (1985). Influence of ammonium ions on calcite and struvite formation byazotobacter in chemically defined media. *Folia Microbiologica.* 30 (1), 55–57. doi: 10.1007/BF02922498

Ronholm, J., Schumann, D., Sapers, H. M., Izawa, M., Applin, D., Berg, B., et al. (2014). A mineralogical characterization of biogenic calcium carbonates precipitated by heterotrophic bacteria isolated from cryophilic polar regions. *Geobiology* 12, 6, 542–556. doi: 10.1111/gbi.12102

Saito, S. (1969). Salt effect on polymer solutions. *J. Polym. Sci. Pol. Chem.* 7 (7), 1789–1802. doi: 10.1002/pol.1969.150070719

Sanz-Saez, I., Pereira-Garcia, C., Bravo, A. G., Trujillo, L., Pla, I. F. M., Capilla, M., et al. (2022). Prevalence of heterotrophic methylmercury detoxifying bacteria across oceanic regions. *Environ. Sci. Technol.* 56 (6), 3452–3461. doi: 10.1021/acs.est.1c05635

Sarayu, K., Iyer, N. R., Annaselvi, M., and Murthy, A. R. (2016). The micro-mechanism involved and wollastonite signature in the calcareous precipitates of marine isolates. *Appl. Biochem. Biotechnol.* 178 (6), 1069–1080. doi: 10.1007/s12010-015-1929-z

Sarmento, H., and Gasol, J. M. (2012). Use of phytoplankton-derived dissolved organic carbon by different types of bacterioplankton. *Environ. Microbiol.* 14 (9), 2348–2360. doi: 10.1111/j.1462-2920.2012.02787.x

Sinha, A., Singh, A., Kumar, S., Khare, S. K., and Ramanan, A. (2014). Microbial mineralization of struvite: A promising process to overcome phosphate sequestering crisis. *Water Res.* 54, 33–43. doi: 10.1016/j.watres.2014.01.039

Spadafora, A., Perri, E., McKenzie, J., and Vasconcelos, C. (2010). Microbial biomineralization processes forming modern Ca:Mg carbonate stromatolites. *Sedimentology.* 57, 27–40. doi: 10.1111/j.1365-3091.2009.01083.x

Sullivan, A. L., and Murdaugh, A. E. (2014). The effects of marine bacteria on barite growth and morphology. *Biophysic. J.* 106 (2), 799a–799a. doi: 10.1016/j.bpj.2013.11.4381

Sun, J. Y., Chen, L., Wang, X. X., Cao, S., Fu, W. J., and Zheng, W. C. (2012). Synthesis of struvite crystals by using bacteria *Proteus mirabilis*. *Synth. Reac. Inorg. M.* 42 (4), 445–448. doi: 10.1080/15533174.2011.611850

Sun, B., Zhao, H., Zhao, Y., Tucker, M. E., Han, Z., and Yan, H. (2020). Bio-precipitation of carbonate and phosphate minerals induced by the bacterium *Citrobacter freundii* ZW123 in an anaerobic environment. *Minerals.* 10 (1), 65. doi: 10.3390/min10010065

Tada, Y., Taniguchi, A., Nagao, I., Miki, T., Uematsu, M., Tsuda, A., et al. (2011). Differing growth responses of major phylogenetic groups of marine bacteria to natural phytoplankton blooms in the western north pacific ocean. *Appl. Environ. Microbiol.* 77 (12), 4055–4065. doi: 10.1128/AEM.02952-10

Torres-Crespo, N., Martinez-Ruiz, F., Gonzalez-Munoz, M. T., Bedmar, E. J., De Lange, G. J., and Jroundi, F. (2015). Role of bacteria in marine barite precipitation: A case study using Mediterranean seawater. *Sci. Total Environ.* 512, 562–571. doi: 10.1016/j.scitotenv.2015.01.044

Tu, Q., Lin, L., Cheng, L., Deng, Y., and He, Z. (2019). NCycDB: a curated integrative database for fast and accurate metagenomic profiling of nitrogen cycling genes. *Bioinformatics.* 35 (6), 1040–1048. doi: 10.1093/bioinformatics/bty741

van de Velde, S. J., Burdorf, L. D. W., Hidalgo-Martinez, S., Leermakers, M., and Meysman, F. J. R. (2022). Cable bacteria activity modulates arsenic release from sediments in a seasonally hypoxic marine basin. *Front. Microbiol.* 13. doi: 10.3389/fmicb.2022.907976

Vigliaturo, R., Marengo, A., Bittarello, E., Perez-Rodriguez, I., Drazic, G., and Giere, R. (2020). Micro- and nano-scale mineralogical characterization of Fe(II)-oxidizing bacterial stalks. *Geobiology.* 18 (5), 606–618. doi: 10.1111/gbi.12398

Wang, X., He, X., Xia, D., Sun, M., An, X., and Lian, B. (2022). The phase transformation of microbial induced struvite and its Cd(II) immobilization mechanism. *J. Environ. Chem. Eng.* 10 (3), 107695. doi: 10.1016/j.jece.2022.107695

Wei, S. P., Cui, H. P., Jiang, Z. L., Liu, H., He, H., and Fang, N. Q. (2015). Biomineralization processes of calcite induced by bacteria isolated from marine sediments. *Brazil J. Microbiol.* 46 (2), 455–464. doi: 10.1590/S1517-838246220140533

Xue, H. P., Zhang, D. F., Xu, L., Wang, X. N., Zhang, A. H., Huang, J. K., et al. (2021). *Actirhodobacter atriluteus* gen. nov., sp. nov., isolated from the surface water of the yellow Sea. *Antonie Van Leeuwenhoek.* 114 (7), 1059–1068. doi: 10.1007/s10482-021-01576-w

Yasumoto-Hirose, M., Yasumoto, K., Iijima, M., Nishino, T., Ikemoto, E., Nishijima, M., et al. (2022). Mg-rich calcite-producing marine bacterium *Pseudovibrio* sp. isolated from an ascidian in coral reefs at Okinawa, Japan. *Fisheries Sci.* 88 (5), 625–634. doi: 10.1007/s12562-022-01627-9

Yoon, J. H., Kang, S. J., and Lee, S. Y. (2012). *Salinimonas lutimaris* sp nov., a polysaccharide-degrading bacterium isolated from a tidal flat. *Antonie Van Leeuwenhoek* 101 (4), 803–810. doi: 10.1007/s10482-011-9695-6

Zhang, Y., and Cremer, P. S. (2006). Interactions between macromolecules and ions: the hofmeister series. *Curr. Opin. Chem. Biol.* 10 (6), 658–663. doi: 10.1016/j.cbpa.2006.09.020

Zhang, D. F., Cui, X. W., Li, W. J., Zhang, X. M., Xue, H. P., Huang, J. K., et al. (2021). Description of *Salinimonas profundi* sp. nov., a deep-sea bacterium harboring a transposon Tn6333. *Antonie Van Leeuwenhoek.* 114 (1), 69–81. doi: 10.1007/s10482-020-01501-7

Zhang, P., Liu, W. P., Zhao, T. L., Yao, Q. Z., Li, H., Fu, S. Q., et al. (2022). Biomineralization of struvite by *Shewanella oneidensis* MR-1 for phosphorus recovery: Cr(VI) effect and behavior. *J. Environ. Chem. Eng.* 10 (1), 106923. doi: 10.1016/j.jece.2021.106923

Zhang, H., Wang, H., Cao, L., Chen, H., Wang, M. X., Lian, C., et al. (2020). *Salinimonas iocasae* sp. nov., a halophilic bacterium isolated from a polychaete tube in a hydrothermal field. *Int. J. Syst. Evol. Microbiol.* 70 (6), 3899–3904. doi: 10.1099/ijsem.0.004258

Zhao, Y., Yan, H., Zhou, J., Tucker, M. E., Han, M., Zhao, H., et al. (2019). Bio-precipitation of calcium and magnesium ions through extracellular and intracellular process induced by *Bacillus licheniformis* SRB2. *Minerals.* 9 (9), 526. doi: 10.3390/min9090526

Zykwinska, A., Berre, L. T., Sinquin, C., Ropartz, D., Rogniaux, H., Colliec-Jouault, S., et al. (2018). Enzymatic depolymerization of the GY785 exopolysaccharide produced by the deep-sea hydrothermal bacterium *Alteromonas infernus*: Structural study and enzyme activity assessment. *Carbohydr. Polym.* 188, 101–107. doi: 10.1016/j.carbpol.2018.01.086